International Journal of Thin Film Science and Technology

Volume 5
Issue 3 *Sep. 2016*

Article 1

2016

DC Conductivity, Thermal Stability and Crystallization Kinetics of the Semiconducting 30P2O5 (50-x)V2O5 xB2O3 20Fe2O3 Oxide Glasses

M. Shapaan
Phys. Dept., Faculty of Science, Al-Azhar Univ., Nasr City, Cairo 11884, Egypt., shapaan100@yahoo.com

International Journal of Thin Films Science and Technology

http://dx.doi.org/10.18576/ijtfst/050301

DC Conductivity, Thermal Stability and Crystallization Kinetics of the Semiconducting $30P_2O_5$ $(50-x)V_2O_5$ xB_2O_3 $20Fe_2O_3$ Oxide Glasses

M. Shapaan[*]

Phys. Dept., Faculty of Science, Al-Azhar Univ., Nasr City, Cairo 11884, Egypt.

Received: 21 Feb. 2016, Revised: 22 Jun. 2016, Accepted: 24 Jun. 2016.
Published online: 1 Sep. 2016.

Abstract: Glasses having compositions $30P_2O_5$ $(50-x)V_2O_5$ xB_2O_3 $20Fe_2O_3$ $(0 \leq x \leq 50)$ mol % are prepared by the normal conventional melt quenching technique. The glassy state of the as prepared glass samples is characterized using X-ray diffraction (XRD) and differential thermal analysis (DTA). The density and molar volume of the investigated glass system decrease with increasing B_2O_3 contents. The room temperature (303 K) dc conductivity is typically 10^{-5} - 10^{-9} (Scm^{-1}) with activation energy 0.30 - 0.46 (eV). Two glass transition temperatures, T_{g1}, and, T_{g2}, are detected at the DTA traces of the investigated glass system. From the dependence on heating rates of, T_{g1}, T_{g2}, and T_p, the activation energies for glass transitions, E_{g1}, E_{g2} and for crystallization, E_c, are calculated. The values determined for Avrami exponent, n, are closed to 3 for the free B_2O_3 glass sample (volume nucleation, two-dimensional growth) and closed to 2 for the other investigated glass samples (volume nucleation, one-dimensional growth).

Keywords: Amorphous semiconductors; Oxide glasses; Thermal stability; Glass transition temperature; Conductivity

1 Introduction

Because of their potential applications in various industrial fields, amorphous materials and glasses are of special scientific and technological interest. Phosphate glasses attract great attention due to their properties such as: low glass transition temperatures, thermal expansion coefficients and glass formation takes place over a wide composition range [1, 2]. The most important class of phosphate based glasses is the one containing transition metal oxides such as Fe_2O_3 and V_2O_5 as an example [3]. Previous studies have shown that, glasses containing transition-metal oxides (TMOs) exhibit semiconducting properties. This behavior may be attributed to the existence of transition-metal ions (TMIs) in more than one valence state [4]. Also it was found that the interaction between electron and phonon in these glasses is strong enough to form small polaron, which contributed to the electrical conduction mechanism through the hopping of small polarons between different valence states as proposed by Austin and Mott [5].

The properties of phosphate based glasses which containing transition metal oxide such as Fe_2O_3 have attracted considerable interest because of their structural, thermal and electric properties. Recent studies of phosphate glasses have shown that the addition of iron has a significant effect on the glass transition temperature, the thermal expansion coefficient and the chemical durability [6, 7]. At the same time studies shown that, dramatically change in the chemical durability of the phosphate based glasses with the addition of Fe_2O_3 which may be attributed to the replacement of P-O-P bonds by more chemically durable P-O-Fe^{2+} and/or P-O-Fe^{3+} bonds [8-10]. The formation of P-O-Fe bonds are responsible for the formation of small polarons and as a result the electric conduction in these glasses occurs by thermally activated small polaron hopping from the low valance state Fe^{2+} (Ferrous ions) to the high valance state Fe^{3+} (Ferric ions) [9].

For vanadium phosphate glasses the same conduction mechanism was found also, where the electric conduction in these glasses may be attributed to small polarons hopping (SPH) which occurs from V^{4+} sites to the neighboring V^{5+} sites [10-13].

The present work aims to study the effect of partial replacement of V_2O_5 glass network modifier (GNM) by B_2O_3 glass former (GF) on the structure, electric conduction, thermal stability and crystallization kinetics of the as quenched $30P_2O_5$ $(50-x)V_2O_5$ xB_2O_3 $20Fe_2O_3$ (x = 0, 10, 20, 30, 40 and 50 mol %) glass system.

[*]Corresponding author E-mail: shapaan100@yahoo.com

2 Experimental Procedures

The glass samples having the general chemical formula $30P_2O_5$ (50-x)V_2O_5 xB_2O_3 20Fe_2O_3 (x = 0, 10, 20, 30, 40 and 50 mol %) have been prepared by the melt quenching technique. The preparation is carried out by melting homogeneous mixtures of reagent grade $NH_4H_2PO_4$, V_2O_5, B_2O_3 and Fe_2O_3 (with purity not less than 99.8 %) in porcelain crucibles using an electric furnace at 1000 ^{0}C for 2 h. The melts are quenched between two pre-cooled copper plates to form (2cmx2cmx2mm) glass samples.

X-ray diffraction patterns are recorded to check for noncrystallinity of the as-quenched glass samples using a Philips X-ray diffractometer PW/1710 with Ni filtered, Cu Kα radiation (λ = 1.542A˚) powered at 40 (kV) and 30 (mA).

The densities of the as prepared glass samples are measured by the suspension weight method based on the Archimedes principle using toluene as an immersion liquid whose density is (0.868 g/cm^3).

The dc conductivity (σ_{dc}) of the as prepared glass samples is measured at the temperature range between 300 and 500 K and under a constant dc voltage. For electric measurements the as prepared glass samples are polished to obtain optically parallel surfaces of 1.5 (mm) thickness. In order to achieve the best electrical contact between the samples and the electrodes of the sample holder the measurements are carried out on the silver paste coated pellets. The value of the current at different temperatures is measured using a picoammeter (Keithley 485 Autoranging Picoammeter) and the *I-V* characteristic between electrodes is verified.

The calorimetric measurements are carried out using differential thermal analysis Shimadzu (50) with an accuracy of ± 0.1 (K). For each heating rate, β, the calorimeter is calibrated using the well - known melting temperatures and melting enthalpies of zinc and indium supplied with the instrument. Twenty milligram powdered of the investigated glass samples, crimped into aluminum pans, and scanned at different heating rates, β, (= 5, 10, 15, 20 and 30 K/min). The values of the glass transition temperature, T_g, the onset temperature of crystallization, T_{cr}, and the crystallization peak temperature, T_p, are determined with accuracy ± 2 (K) by using the microprocessor of the thermal analyzer.

3 Results and Discussion

3. 1 Density and molar volume

The variation of the density of the investigated glass samples as a function of B_2O_3 mol % can be expressed in terms of apparent volume occupied by 1g atom of oxygen molar volume, V_m, which can be calculate from the room temperature measured density and composition using the following relation[14];

$$V_m = \sum(n_i M_w)/\rho \quad (1)$$

where, M_w, is the molecular weight of oxide, n_i, is the molar fraction and, ρ, is the density of the investigated glass sample. Fig. 1 shows the variation of the density and molar volume of the $30P_2O_5$ (50-x)V_2O_5 xB_2O_3 20Fe_2O_3 (x = 0, 10, 20, 30, 40 and 50 mol %) glass system as a function of B_2O_3 contents. From the density measurements of all the $30P_2O_5$ (50-x)V_2O_5 xB_2O_3 20Fe_2O_3 (x = 0, 10, 20, 30, 40 and 50 mol %) glass samples it is found that, the density, ρ, decreases with increasing B_2O_3 contents as shown in Fig. 1(a). The relative error in these measurements is about ± 0.01 (g/cm^3). Fig. 1(b) shows the variation of the molar volume, V_m, as a function of B_2O_3 contents. It is found that, V_m, decreases with increasing B_2O_3 contents. The decrease of the density with increasing B_2O_3 contents may be due to the lower molecular mass of B_2O_3 when compared to the higher molecular mass of V_2O_5. Similar behavior was found for some oxide glasses containing B_2O_3 [15-17]. The values of the density, ρ, and molar volume, V_m, are listed in Table 1.

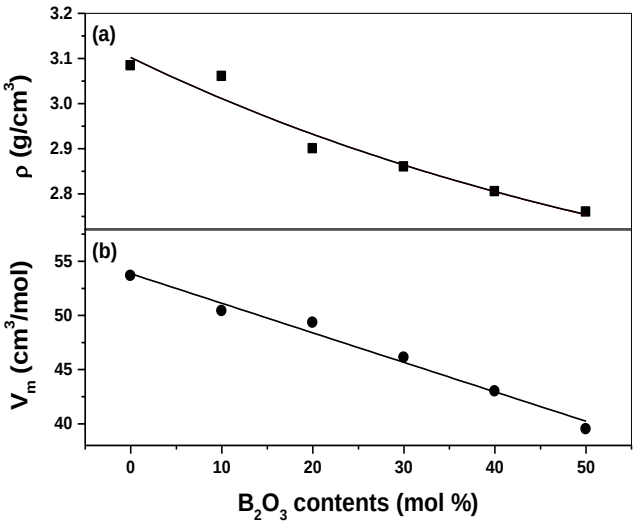

Fig. 1. Density, ρ, and molar volume, V_m, of the $30P_2O_5$ (50-x)V_2O_5 xB_2O_3 20Fe_2O_3 (x = 0, 10, 20, 30, 40 and 50 mol %) glass system as a function of B_2O_3 contents.

3.2 Dc conductivity measurements

The effects of temperature and the partial replacement of V_2O_5 by B_2O_3 on the dc electric conductivity are studied in more details. The temperature dependence of the dc electrical conductivity, σ_{dc}, of the $30P_2O_5$ (50-x)V_2O_5 xB_2O_3 20Fe_2O_3 (x = 0, 10, 20, 30, and 40 mol %) glass

samples is measured. Fig. 2 shows ln(σ_{dc}) vs. 1/T [K^{-1}] of the investigated glass samples. It is clear from this Figure that the dc conductivity increase with increasing temperature and decreasing with the partial replacement of V_2O_5 by B_2O_3 in the composition. Also it is found that the general behavior of the dc conductivity with temperature is straight line over the temperature range from 300 to 500 (K). The temperature dependence of the dc conductivity, σ_{dc}, obeys Arrhenius relationship;

$$\sigma_{dc} = \sigma_0 \, exp[-E_{dc}/k_B T] \quad (2)$$

where, E_{dc}, is the activation energy for conduction, σ_0, is the pre-exponential factor, k_B, is the Boltzmann constant and, T, is the absolute temperature in (K). The activation energies of the investigated glass samples are determined from the slope of ln(σ_{dc}) vs. 1/T. The activation energies are then evaluated by least squares fitting method of eq. (2). Fig. 3(a) shows the variation of the dc conductivity of the investigated glass samples at different temperatures (303, 393 and 463 K) as an example and Fig. 3(b) shows the variation of the activation energy as a function of composition (B_2O_3 mol %). It is found that the dc conductivity, σ_{dc}, increase with increasing temperature and decreases with increasing B_2O_3 contents.

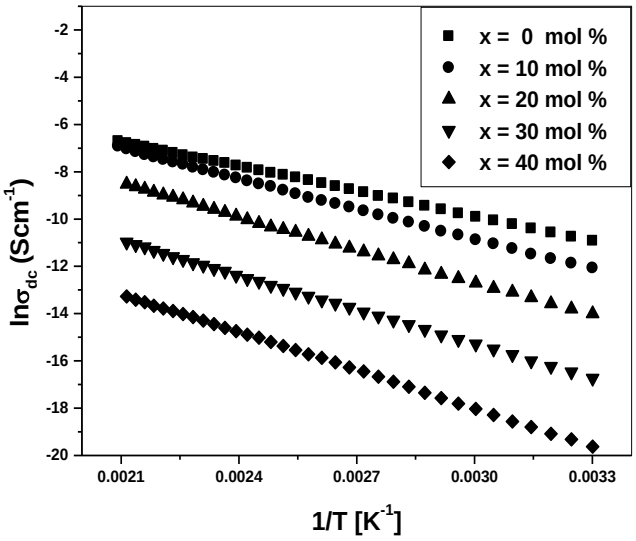

Fig. 2. Plots of ln(σ_{dc}) vs. 1/T [K^{-1}] of the $30P_2O_5$ (50-x)V_2O_5 xB_2O_3 $20Fe_2O_3$ (x = 0, 10, 20, 30, and 40 mol %) glass samples.

The increase of the dc conductivity with increasing temperature may be attributed to the increase of the thermally activated small polarons hopping (SPH) [18, 19]. The values of, σ_{dc}, for the free B_2O_3 glass sample ($30P_2O_5$ $50V_2O_5$ $20Fe_2O_3$) are $1.8x10^{-5}$, $2.63x10^{-4}$ and $9.72x10^{-4}$ (Scm^{-1}) at temperatures 303, 393 and 463 (K) respectively (as an example). The decreasing in the dc conductivity with the partial replacement of V_2O_5 by B_2O_3 can be attributed to the decrease of the transition metal oxide (TMO) in the composition and as a result decreasing the number of small polarons hopping (SPH) which contributed to the electric conduction [18, 19]. On the other hand the conduction mechanism of the present amorphous semiconductor system depends mainly on the electron hopping from V^{4+} sites to the neighboring V^{5+} sites. The vanadium ions play the role of glass network modifier (GNM) and the electric conduction in this glass system can be attributed to small polarons hopping (SPH) [12, 13]. Generally, it is known that, the decreasing in the dc conductivity with decreasing vanadium oxide can be attributed to decrease of non-bridging oxygen. The room temperature dc conductivity of the investigated glass system is typically $1.8x10^{-5}$ - $2.99x10^{-9}$ (Scm^{-1}) with activation energy 0.30 - 0.46 (eV). At the same time as shown in Figure 3 the decreases of the dc conductivity and increases the activation energy with increasing B_2O_3 contents may be due to decrease of the density of the localized states in the band gab near the Fermi level of the semiconducting glass samples. The obtained results are in good agreement with the already available results for different semiconducting glasses [20, 21]. The values of the dc conductivity, σ_{dc}, at different temperatures (303, 393 and 463 K) and activation energies, E_{dc}, of the investigated glass samples are listed in Table 1.

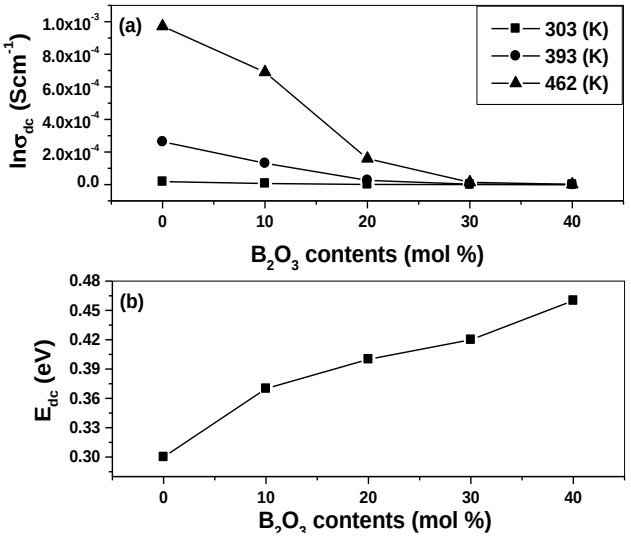

Fig. 3. (a) - Dc Conductivity as a function of B_2O_3 contents at different temperatures (303, 393 and 463 K) of the $30P_2O_5$ (50-x)V_2O_5 xB_2O_3 $20Fe_2O_3$ (x = 0, 10, 20, 30, and 40 mol %) glass samples. (b) - The activation energies of the investigated glass samples as a function B_2O_3 contents.

3.3 Thermal analysis and thermal stability of glasses

Using DTA the thermal stability of the investigated glass system is studied in more details. All the investigated glass samples exhibit two endothermic minima, T_{g1} and T_{g2}.

The first endothermic minima represent the glass transition temperature, T_{g1}, which confirm the glassy nature of the investigated samples. The second endothermic minima, T_{g2}, may be attributed to the ferroelectric transition temperature [13]. Fig. 4 shows the DTA traces of the $30P_2O_5$ (50-x)V_2O_5xB_2O_3 $20Fe_2O_3$ (x = 0, 20 and 40 mol %) glass samples at 20 (K/min) heating rate, β, as an example. The glass samples with x = 0, 10 and 20 (mol %) exhibit two glass transition temperatures followed by one crystallization peak. Also for the glass samples x = 40 and 50 (mol %) two glass transition temperatures are detected but followed by two crystallization peaks.

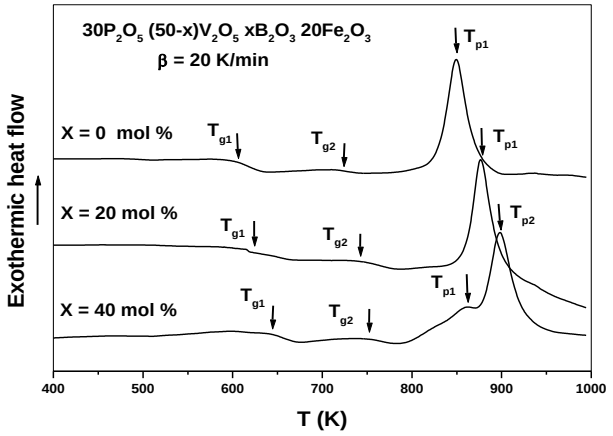

Fig. 4. Typical DTA traces of the $30P_2O_5$ (50-x)V_2O_5 xB_2O_3 $20Fe_2O_3$ (x = 0, 20 and 40 mol %) glass samples at 20 (K/min) heating rate.

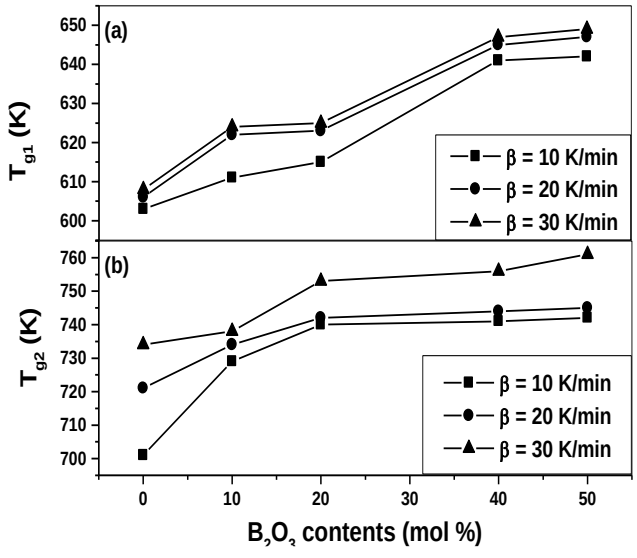

Fig. 5. (a and b) - Glass transition temperatures, T_{g1}, and, T_{g2}, as a function of B_2O_3 at different heating rate (β = 10, 20 and 30 K/min).

Fig. 5(a and b) shows the variation of the glass transition temperatures, T_{g1}, and, T_{g2}, as a function of B_2O_3 contents at different heating rates (β = 10, 20 and 30 K/min). It is found that, the glass transition temperatures, T_{g1}, and, T_{g2}, are shifted to higher temperatures with increasing B_2O_3 contents. The increase in the glass transition temperatures as a function of B_2O_3 contents may be due to the replacement of the weaker O-V-O linkages by strong V-O-B and O-B-O linkages [22-24] indicates strengthening of the glass network as V_2O_5 is replaced by B_2O_3. The same behavior of the glass transition temperature, T_g, as a function of V_2O_5 contents was found in previous studies of several vanadate glasses [25-27].

The activation energies of enthalpy relaxation of the glass transitions, E_{g1}, and, E_{g2}, can be determined using the Kissinger formula which, was originally derived for the crystallization process and suggested to be valid for the glass transition [28-30]. This formula has the following form;

$$ln(T_g^2/\beta) = E_g/RT_g + const. \quad (3)$$

where R is the universal gas constant, T_g, is the glass transition temperature, E_g, is the glass transition activation energy and, β, is the heating rate. The values of the glass transition activation energies, E_{g1}, and, E_{g2}, can be estimated from $\ln(T_{g1}^2/\beta)$ vs. $1000/T_{g1}$ and $\ln(T_{g2}^2/\beta)$ vs. $1000/T_{g2}$ as shown in Fig. 6(a and b) respectively. The values of the glass transition activation energies, E_{g1}, and, E_{g2}, are evaluated by least squares fitting method of eq. (3) and the solid lines are guides for eyes.

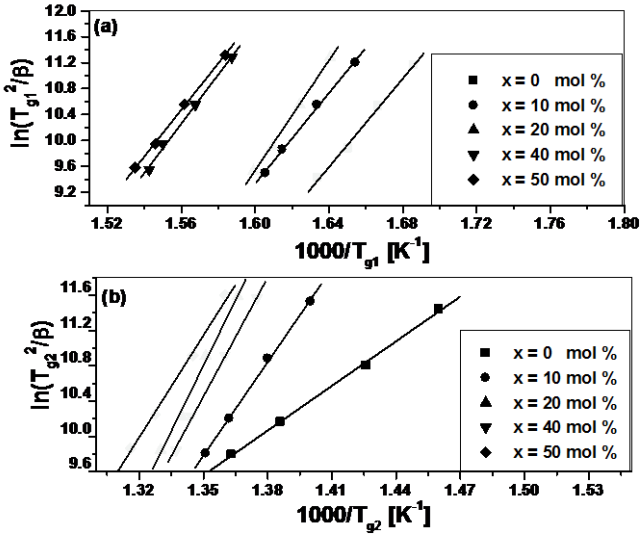

Fig. 6. Plots of (a) - $\ln(T_{g1}^2/\beta)$ vs. $1000/T_{g1}$ and (b) - $\ln(T_{g2}^2/\beta)$ vs. $1000/T_{g2}$ of the as quenched $30P_2O_5$ (50-x)V_2O_5 xB_2O_3 $20Fe_2O_3$ (x = 0, 10, 20, 40 and 50 mol %) glass samples.

The dependence of the glass transition temperature, T_g, on the heating rate, β, have been studied using two approaches. The first approach regarding the dependence of the glass transition temperature on the heating rate is based on Kissinger's method [28]. The second approach to determine the glass transitions activation energies, E_{g1} and, E_{g2}, is based on a simplified form of eq. (3). According to Mahadevan et al. [31] Kissinger equation was simplified to the following form [29-31];

$$ln(\beta) = -E_g/RT_g + const. \quad (4)$$

This formula has been used to calculate, E_{g1}, and E_{g2}, as shown in Fig. 7(a and b) respectively. The values of the glass transition activation energies, E_{g1}, and, E_{g2}, is evaluated by least squares fitting method of eq. (4) and the solid lines are guides for eyes.

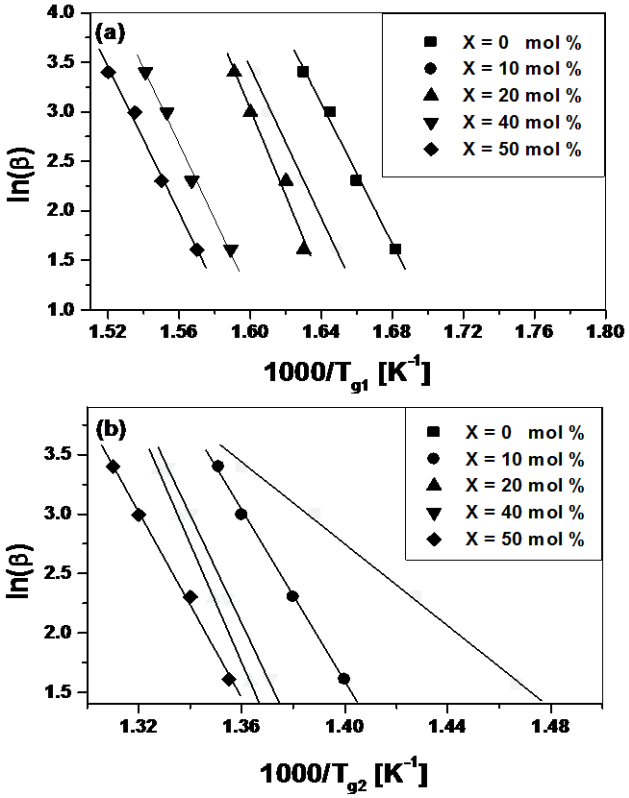

Fig. 7. Plots of (a) - ln(β) vs. $1000/T_{g1}$ and (b) - ln(β) vs. $1000/T_{g2}$ of the as quenched $30P_2O_5$ (50-x)V_2O_5 xB_2O_3 $20Fe_2O_3$ (x = 0, 10, 20, 40 and 50 mol %) glass samples.

Fig. 8 shows the variation of the glass transition activation energies, E_{g1}, and, E_{g2}, as a function of B_2O_3 contents. As shown in this Figure the glass sample with x = 20 (mol %) has the highest values of, E_{g1}, and, E_{g2}. From Kissinger analysis, the values of, E_{g1}, and, E_{g2}, of the glass sample with x = 20 (mol %) are 353 and 412 ± 3 (kJ/mol) respectively. Also from Mahadevan et al. analysis, the values of, E_{g1}, and, E_{g2}, of the glass sample with x = 20 (mol %) are 363 and 423 ± 3 (kJ/mol) respectively.

For the evaluation of activation energy of crystallization, E_c, by using the variation of crystallization peak temperature, T_p, with heating rate, β, Vazquez et al. [32] developed the proposed method by Kissinger [28] for non-isothermal analysis of diversification as follows;

$$ln\left(\frac{T_p^2}{\beta}\right) = \frac{E_c}{RT_p} + ln\left(\frac{E_c}{Rk_0}\right) \quad (5)$$

Fig. 9(a) shows the relation $ln(T_p^2/\beta)$ vs. $1000/T_p$ of the as quenched $30P_2O_5$ (50-x)V_2O_5 xB_2O_3 $20Fe_2O_3$ (x = 0, 10 and 20 mol %) glass samples. Fig. 9(b) shows the relation $ln(T_p^2/\beta)$ vs. $1000/T_p$ of the as quenched $30P_2O_5$ (50-x)V_2O_5 xB_2O_3 $20Fe_2O_3$ (x = 40 and 50 mol %) glass samples.

From the slope of the straight line fitting of the experimental data the crystallization activation energy, E_c, is evaluated by the least squares fitting method of eq. (5) and the solid lines are guides for eyes.

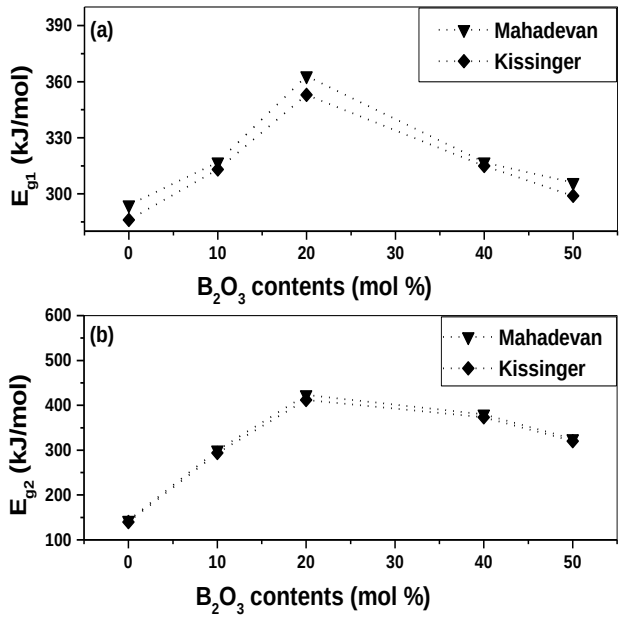

Fig. 8. Glass transition activation energies, E_{g1}, and, E_{g2}, as a function of B_2O_3 contents.

Fig. 10(a) shows the variation of the crystallization activation energy, E_c, of the as prepared glass samples as a function of B_2O_3 contents. It is found that E_c, increases with increasing B_2O_3 contents up to 20 (mol %) and decrease after this concentration. Fig. 10(b) shows the variation of the thermal stability criteria, $\Delta T_x = T_{cr} - T_g$ [33] as a

function of B_2O_3 contents. The thermal stability criteria, $\Delta T_x = T_{cr} - T_g$, is a rough measure of the glass thermal stability, where, T_{cr}, is the onset temperature of crystallization, so the larger differences between, T_{cr}, and, T_g, indicating more thermal stable glasses. The thermal stability criteria, ΔT_x, increases with increasing B_2O_3 contents up to 20 (mol %) and decrease after this concentration. This meaning that, the thermal stability increases up to 20 (mol %) of B_2O_3 and decreases after this concentration [15].

At the same time as shown in Fig. 10 direct relation could be observed between the crystallization activation energy, E_c, (nucleation barrier) and the thermal stability criteria, ΔT_x. From the last results one can see that, the glass sample with x = 20 (mol %) has the highest values of the, E_{g1}, E_{g2}, E_c, and, ΔT_x, and this confirmed that, this glass sample is of the highest thermal stability against crystallization among all the investigated glass samples.

The thermal transition data (T_{g1}, T_{g2}, T_{cr}, and T_p), the thermal stability criteria, ΔT_x, at 10 K/min heating rate (as an example) the crystallization activation energy, E_c, and the pre. exp. factor, k_0, are listed in Table 2.

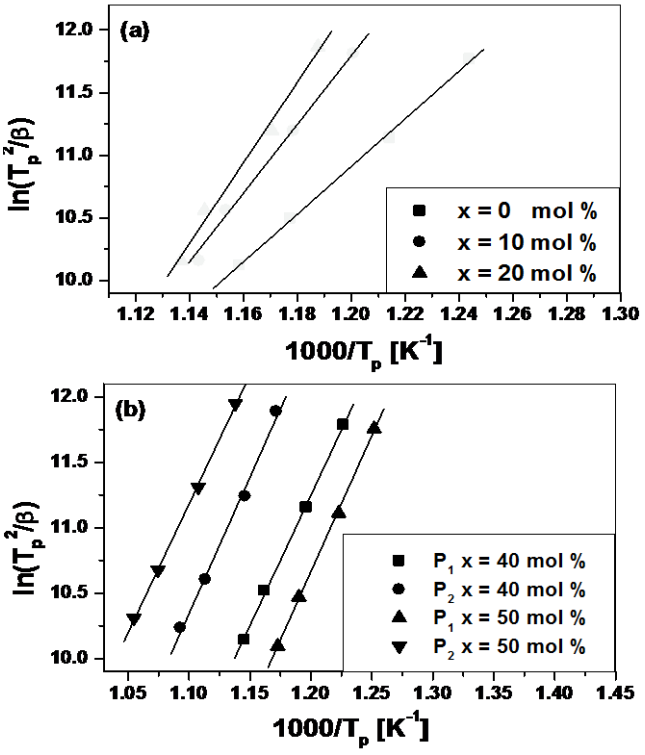

Fig. 9. (a) - Plots of $\ln(T_p^2/\beta)$ vs. $1000/T_p$ of the as quenched $30P_2O_5$ $(50\text{-}x)V_2O_5$ xB_2O_3 $20Fe_2O_3$ (x = 0, 10, 20 mol %) and (b) - Plots of $\ln(T_p^2/\beta)$ vs. $1000/T_p$ of the as quenched $30P_2O_5$ $(50\text{-}x)V_2O_5$ xB_2O_3 $20Fe_2O_3$ (x = 40 and 50 mol %) glass samples.

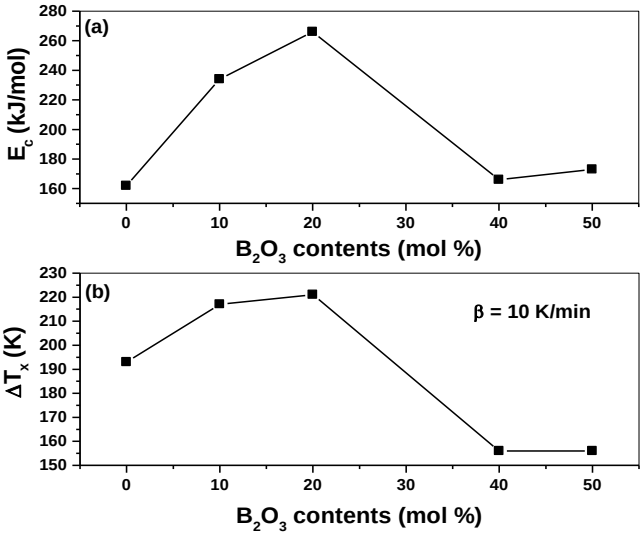

Fig. 10. Crystallization activation energy, E_c, and the thermal stability criteria, ΔT_x, as a function of B_2O_3 contents.

3.4 Crystallization kinetics and kinetic exponent

The crystallization fraction, χ, can be expressed as a function of time according to the Johnson - Mehl -Avrami equation [34-36];

$$\chi(t) = 1 - exp[-(kt)^n] \quad (6)$$

where, n, is the Avrami exponent which depends on the mechanism of the growth and dimensionality of crystal growth and, k, is defined as the reaction rate constant and is given by the following formula;

$$k = k_0\, exp(-E_c/RT) \quad (7)$$

where, E_c, is the activation energy of crystallization, R, is the universal gas constant, T, is the isothermal temperature and, k_0, is the frequency factor. For the non-isothermal method the theoretical basis for interpreting DTA results is provided by the formal theory of transformation kinetics, which was developed by Johnson et al. [34] and Avrami [35, 36]. The crystallization fraction, χ, at a given temperature, T, is given by, $\chi = A_T/A$, where, A, is the total area of the exothermic peak between the temperatures, T_i, and, T_f, and, A_T, is the area between, T_i and T, as shown in Fig. 11. The temperatures, T_i, and, T_f, are the crystallization is just beginning temperature and the crystallization is completed temperature respectively.

The graphical representation of the volume fraction of crystallization of the investigated glass samples at different heating rate, β, is shown typical sigmoid curve as a function of temperature in crystallization reactions [37, 38]. The crystallization rate is given from the ratio between the

ordinates of the DTA curve and the total area of the peak from which it is possible to build the curves of the exothermic peaks. It is found that the values of $(d\chi/dt)_p$ increase with increasing heating rate, β, which is a property that has been widely discussed in the literature [37-39]. The kinetic exponent, n, can calculate from the experimental values of $(d\chi/dt)_p$ using the following equation [40-42];

$$(d\chi/dt)_p = n(0.37\beta E_c)/(RT_p^2) \quad (8)$$

The kinetic exponent, n, was deduced on the basis of the mechanism of crystallization [43]. From the average value of the kinetic exponent, n, it is possible to postulate a crystallization reaction mechanism for the $30P_2O_5$ $(50\text{-}x)V_2O_5$ xB_2O_3 $20Fe_2O_3$ (x = 0, 10, 20, 40 and 50 mol %) glass samples. Mahadevan et al. [31] shown that the kinetic exponent, n, may be 4, 3, 2 or 1, which are related to different glass-crystal transformation mechanism: n = 4, volume nucleation, three-dimensional growth; n = 3, volume nucleation, two-dimensional growth; n = 2, volume nucleation, one-dimensional growth; n = 1, surface nucleation, one-dimensional growth from surface to the inside. The kinetic exponent, n, of the investigated glass system for each of the experimental heating rates is found to be closed to 2 (n~2) except for the free B_2O_3 glass sample, n, is closed to 3 (n~3). This means that, the growth kinetics of the free B_2O_3 glass sample is volume nucleation, two-dimensional growth and the growth kinetics of the glass samples with (x = 10, 20, 40 and 50 mol %) is volume nucleation, one-dimensional growth.

The maximum crystallization rate, (dχ/dt), the kinetic exponent, n, of the glass samples with (x = 0, 10, 20, 40 and 50 mol %) at 10 K/min heating rate (as an example) and the average kinetic exponent $\langle n \rangle$ are listed in Table 3. To confirm the last results for the crystallization activation energy, E_c, which calculated from eq. (5) and Avrami exponent, n, which calculated from eq. (8) the next approach applied by Matusita et al. [44] for non-isothermal crystallization process. This approach state that the volume fraction of crystallites, χ, precipitated at a given temperature, T, in a glass heated at constant rate, β, can be related to the activation energy of crystallization, E_c, and to the Avrami exponent, n, through the following expression [44];

$$ln[-ln(1-\chi)] = -n\,ln(\beta) - 1.052m\left(\frac{E_c}{RT}\right) + const \quad (9)$$

where *n* is the Avrami exponent depending on the nucleation process and *m* is an integer which depends on the dimensionality of the crystal. Where $n = m + 1$ is taken for as quenched glass containing no nuclei and $n = m$ for a preheated glass containing sufficiently large number of nuclei [29, 30].

Fig. 12 show plots of ln[−ln(1− χ)] vs. ln(β) at four fixed temperatures for the $30P_2O_5$ $(50\text{-}x)V_2O_5$ xB_2O_3 $20Fe_2O_3$ glass samples with (x = 0, 10 and 20 mol %). The values of Avrami exponent, n, are determined from the slope of these curves at each temperature. It is found that, the average value of Avrami exponent, n, for the free B_2O_3 glass sample (x = 0 mol %) is 2.8 closed to 3 (n~3) and m = 2 which meaning that, the growth kinetics of the investigated glass sample with x = 0 (mol %) is volume nucleation, two-dimensional growth. Also it is found that the average values of Avrami exponent, n, of the glass samples with x =10 and 20 (mol %) are 2.25 and 2.33 respectively. These results revealed that, the average values of Avrami exponent, n, closed to 2 (n~2) and m = 1 this meaning that, the growth kinetics of the investigated glass samples with x = 10 and 20 (mol %) is volume nucleation, one-dimensional growth.

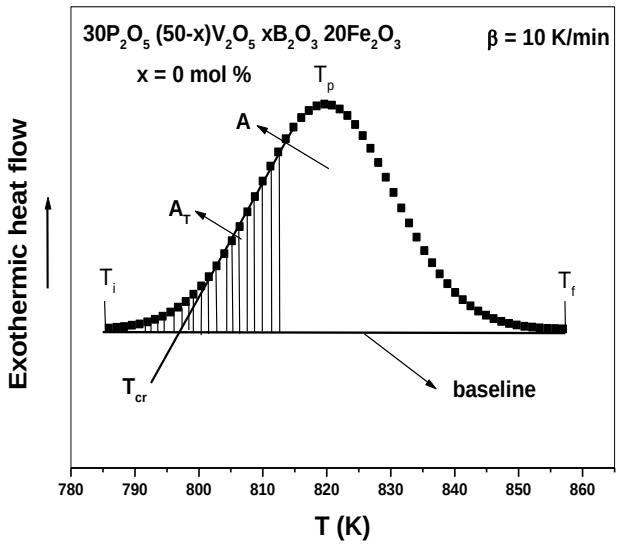

Fig. 11. DTA traces for $30P_2O_5$ $(50\text{-}x)V_2O_5$ xB_2O_3 $20Fe_2O_3$ glass sample x = 0 (mol %) at 10 (K/min) heating rate; the lined area, A_T, shows between, T_i, and, T_f, of the peak. T_i, T_f, and, T, are according to the text.

Fig. 13 show the plots ln[-ln(1-χ)] vs. 1000/T [K^{-1}] of the glass samples with x = (0, 10 and 20 mol %) and it is cleared from this Figure that, these plots are not straight lines. This suggests that, there is a variation in, E_c, and, n, during the crystallization process of glass [45, 46]. According to some previous articles the crystallization activation energy for different crystallization volume fractions is not constant in the whole transformation due to the change of nucleation and growth behaviors during the crystallization process [46].

The variation of the activation energy, E_c, and Avrami exponent, n, can be expressed by the local activation energy, $E_c(\chi)$, and the local Avrami exponent, n(χ), [45, 47, 48]. From non-isothermal DTA results the local activation energy, $E_c(\chi)$, is determined using the proposed method by Ozawa according to the following equation [49, 50];

$$\left[\frac{d(ln\,(\beta))}{d(1/T)}\right]_\chi = -\frac{E_c(\chi)}{R} \quad (10)$$

Fig. 14 show the plots of ln(β) vs. 1000/T [K^{-1}] at various values of, χ, ($0.1 < \chi < 0.9$) for the glass samples with x = 10 and 20 (mol %) (as an example). From the slopes the local activation energies, $E_c(\chi)$, are calculated as a function of crystallization fraction, χ. From the calculated values of the local activation energies, $E_c(\chi)$, for a non-isothermal crystallization process the local Avrami exponents, n(χ), are determined as a function of crystallization fraction, χ, using the following equation [29, 45, 51];

$$n(\chi) = -\frac{R}{E_c(\chi)}\left(\frac{\partial[\ln(-\ln(1-\chi))]}{\partial(1/T)}\right) \qquad (11)$$

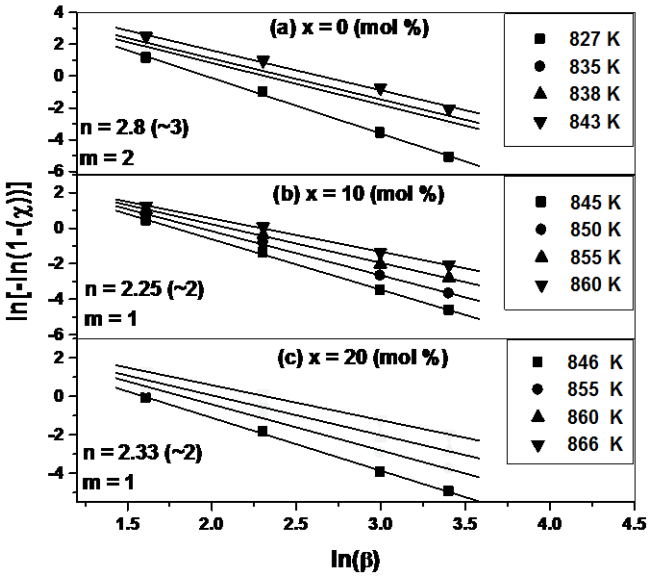

Fig. 12. Plots of ln[−ln(1− χ)] vs. ln(β) at different fixed temperatures for $30P_2O_5$ (50-x)V_2O_5 xB_2O_3 20Fe_2O_3 glass samples with x = 0, 10 and 20 (mol %).

Fig. 15 shows the change of, $E_c(\chi)$, as a function of crystallization fraction, χ, and, n(χ), as a function of crystallization fraction, χ, at 10 (K/min) heating rate of the glass samples with x = 0, 10 and 20 (mol %). For the glass sample with x = 0, 10 and 20 (mol %) it is found that the local activation energies at the initial stage of crystallization process (χ = 0.1) are equal to 211, 275 and 307 ± 3 (kJ/mol) which decrease slowly until 155, 230 and 252 ± 3 (kJ/mol) for, χ = 0.9 respectively.

The mean values of, $E_c(\chi)$, for the glass samples with x = 0, 10 and 20 (mol %) are 183, 252.5 and 279.5 (kJ/mol) respectively. These results are in a good agreement with the results which calculated from Kissenger equation (eq. 5) for the crystallization activation energy, E_c, which are equal to 162, 234 and 266 ± 3 (kJ/mol) for the glass samples with x = 0, 10 and 20 (mol %) respectively. Also it is found that, the mean values of the local Avrami exponent, n(χ), of the investigated glass samples are 3.05, 2.40 and 2.25 respectively. This meaning that, the local Avrami exponent, n(χ), closed to 3 and m = 2 for the glass sample with x = 0 (mol %) and closed to 2 and m = 1 for the glass samples with x = 10 and 20 (mol %). These results are in a good agreement with the average values of Avrami exponent $\langle n \rangle$ which calculated from eq. (8) (Table 3) and which calculated from eq. (9).

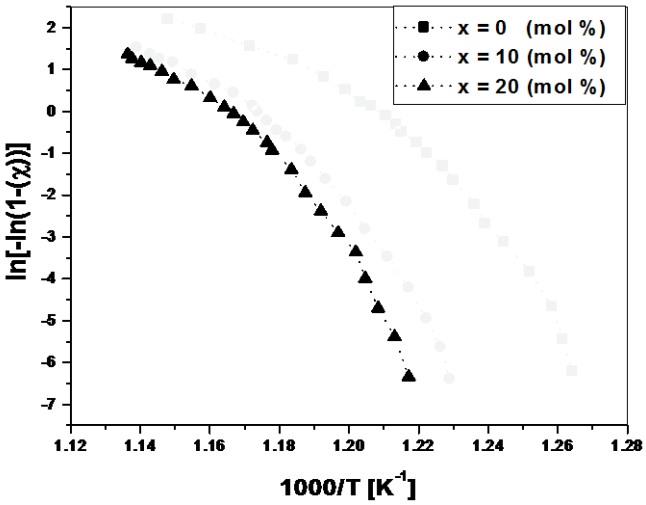

Fig. 13. Plots of ln[−ln(1−χ)] vs.1000/T [K^{-1}] for the glass samples $30P_2O_5$ (50-x)V_2O_5 xB_2O_3 20Fe_2O_3 with x = 0, 10 and 20 (mol %).

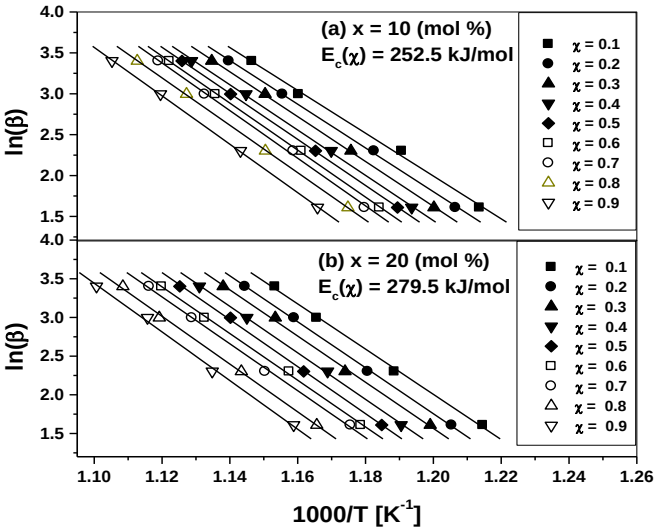

Fig. 14. Plots of ln(β) vs. 1000/T [K^{-1}] at various values of, χ, ($0.1 < \chi < 0.9$) for $30P_2O_5$ (50-x)V_2O_5 xB_2O_3 20Fe_2O_3 glass samples with x = 10 and 20 (mol %).

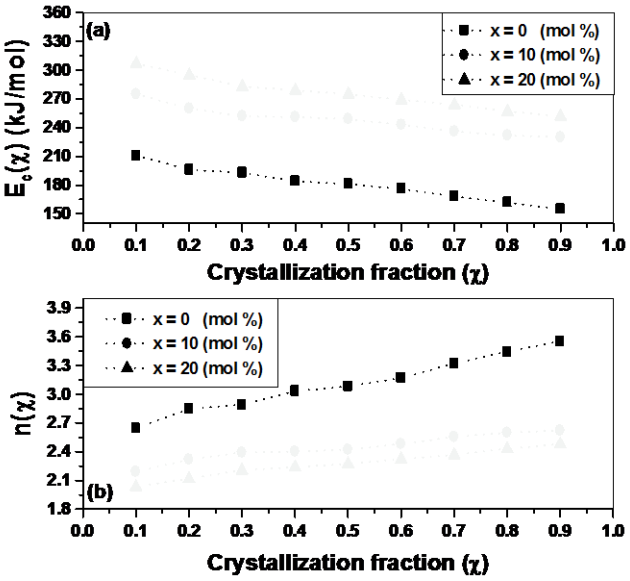

Fig. 15. (a) - Local activation energy for crystallization, $E_c(\chi)$, and (b) - Local Avrami exponent, $n(\chi)$, as a function of crystallization fraction, χ, at 10 K/min heating rate for $30P_2O_5$ (50-x)V_2O_5 xB_2O_3 $20Fe_2O_3$ glass samples with x = 0, 10 and 20 (mol %).

Table 1. Density, ρ, Molar volume, V_m, Dc conductivity, σ_{dc}, at different temperatures (303, 393 and 463 K) and activation energy, E_{dc}, of the $30P_2O_5$ (50-x)V_2O_5 xB_2O_3 $20Fe_2O_3$ glass samples with (x = 0, 10, 20, 30, and 40 mol %).

B_2O_3 (mol %)	Density D (g/cm^3)	Molar volume V_M (cm^3/mol)	σ_{dc} (Scm^{-1}) 303 (K)	σ_{dc} (Scm^{-1}) 393 (K)	σ_{dc} (Scm^{-1}) 463 (K)	E_{dc} (eV) ± 0.011
x = 0.0	3.08	53.66	1.80x10^{-5}	2.63x10^{-4}	9.72x10^{-4}	0.30
x =10	3.06	50.40	6.70x10^{-6}	1.31x10^{-4}	6.90x10^{-4}	0.37
x = 20	2.90	49.33	8.29x10^{-7}	2.59x10^{-5}	1.59x10^{-4}	0.40
x = 30	2.86	46.10	5.37x10^{-8}	2.03x10^{-6}	1.38x10^{-5}	0.42
x = 40	2.81	43.00	2.99x10^{-9}	1.77x10^{-7}	1.34x10^{-6}	0.46

Table 2. The values of thermal transition parameters; glass transition temperatures, T_{g1}, and, T_{g2}, onset temperature of crystallization, T_{cr}, crystallization peak temperature, T_p, thermal stability criteria, ΔT_x, at 10 K/min heating rate, β, the crystallization activation energy, E_c, and Pre-exp. factor, k_0, of $30P_2O_5$ (50-x)V_2O_5 xB_2O_3 $20Fe_2O_3$ glass system.

B_2O_3 (mol %)	β (K/min)	T_{g1} (±2K)	T_{g2} (±2K)	T_{cr} (±2K)	T_p (±2K)	ΔT_x (K)	E_c ±3(kJ/mol)	Pre-exp. factor, k_0 (S^{-1})
x = 0.0	10	603	701	796	819	193	162	7.92E+7
x = 10	10	611	729	828	848	217	234	11.54E+12
x = 20	10	615	740	836	853	221	266	6.62E+13
x = 40 (First peak)	10	641	741	797	836	156	166	1.21E+8
x = 40 (Sec. peak)	10				873		174	1.08E+8
x = 50 (First peak)	10	642	742	798	818	156	173	5.73E+8
x = 50 (Sec. peak)	10				903		164	5.43E+8

Table 3. Maximum crystallization rate (dχ/dt), kinetic exponent, n, at 10 K/min heating rate, β, and average kinetic exponent $\langle n \rangle$ of $30P_2O_5$ (50-x)V_2O_5 xB_2O_3 $20Fe_2O_3$ glass system.

B_2O_3 (mol %)	B (K/min)	(dχ/dt) X 10^{-3} s^{-1}	n	<n>
x = 0.0	10	4.78	2.57	2.58
x = 10	10	4.66	1.908	1.91
x = 20	10	4.14	1.533	1.55
x = 40 (First peak)	10	3.79	2.113	2.10
x = 40 (Second Peak)	10	3.78	2.214	2.21
x = 50 (First peak)	10	3.76	1.909	1.90
x = 50 (Second Peak)	10	3.67	2.408	2.41

4 Conclusions

The effect of partial replacement of V_2O_5 by B_2O_3 on the density, molar volume, dc conductivity, thermal stability and crystallization kinetics of the $30P_2O_5$ (50-x)V_2O_5 xB_2O_3 $20Fe_2O_3$ (x = 0, 10, 20, 30, 40 and 50 mol %) glass system is studied in more details. It is found that the density and the molar volume are decrease with increasing B_2O_3 contents. The dc electrical conductivity, σ_{dc}, decreases with decreasing V_2O_5 contents (TMO). From the DTA results it is found that, the glass transition temperature, T_g, increase with the partial replacement of V_2O_5 by B_2O_3 which indicating the strengthening of glass network. At the same time it is found that, the activation energy of crystallization, E_c, (nucleation barrier) is directly related to the width of the super-cooled liquid region, ΔT_x. The glass sample with x = 20 (mol %) has the highest values of the, E_{g1}, E_{g2}, E_c, and, ΔT_x, and this confirmed that this glass sample is of the highest thermal stability of the investigated glass system. The growth kinetics of the free B_2O_3 glass sample is volume nucleation, two-dimensional growth (n~3) and the growth kinetics of the glass samples with x = 10, 20, 40 and 50 (mol %) is volume nucleation, one-dimensional growth (n~2).

References

[1] J.J. Hudgens, R.K. Brow, D.R. Tallant, S.W. Martin, J. Non-Cryst. Solids 223 (1998) 21.

[2] C.G.S. Pillai, V. Sudarsan, M. Roy, A.K. Dua, J. Non-Cryst. Solids 321 (2003) 313.

[3] A. Chahine, M. Et-tabirou, J.L. Pascal, Mater. Lett. 58 (2004) 2776.

[4] N.F. Mott, J. Non-Cryst. Solids 1 (1968) 1.

[5] I.G. Austin, N.F. Mott, Advances in Physics, 18 (1969) 41.

[6] A. Moguš-Milanković, A. Šantić, A. Gajović, D.E. Day, J. Non-Cryst. Solids 325 (2003) 76.

[7] S.T. Reis, D.L.A. Faria, J.R. Martinelli, W.M. Pontuschka, D.E. Day, C.S.M. Partini, J. Non-Cryst. Solids 304 (2002) 189.

[8] X. Yu, D.E. Day, G.J. Long, R.K. Brow, J. Non-Cryst. Solids 215 (1997) 21.

[9] L. Baia, R. Stefan, W. Kiefer, J. Popp, S.J. Simon, J. Non-Cryst. Solids 303 (2002) 379.

[10] L. Montagne, G. Palavit, G. Mairesse, Phys. Chem. Glasses 37 (1996) 206.

[11] B. Santic, A. Mougs-Miliankovic, D. E. Day, J. Non-Cryst. Solids 296 (2001) 65.

[12] M. Shapaan, E.R. Shabaan, A.G. Mostafa, Physica B 404 (2009) 2058.

[13] M. Shapaan, J. Non-Cryst. Solids 356 (2010) 314.

[14] Dorina Rusu, I. Ardelean, Materials Research Bulletin 43 (2008) 1724.

[15] M. Shapaan, F.M. Ebrahim, Physica B 355 (2009) 926.

[16] Syed Rahman Shashidhar Bale, A.M. Awasthi, V. Sathe, J. Alloys Compd. 460 (2008) 699.

[17] El-Sayed Moustafa, Yasser B. Saddeek, Essam R. Shaaban, J. Phys. Chem. Solids 69 (2008) 2281.

[18] L. Murawski, R.J. Barczynski, Solid State Ionics 176 (2005) 2145.

[19] S. Sindhu, S. Sanghi, A. Agarwal, Sonam, V.P. Seth, N. Kishore, Physica B 365 (2005) 65.

[20] M.M. El-Desoky, M.Y. Hassaan, Phys. Chem. Glasses 43 (2002) 1.

[21] H.El-Mkami, B. Deroide, R. Backov, J.V. Zanchetto, J. Phys. Chem. Solids 61 (2000) 819.

[22] S. Muthupari, S. Prabakar, K.J. Rao, J. Phys. Chem. 98 (1994) 2646.

[23] Huaxin Li, Huixing Lin, Wei Chen, Lan Luo, J. Non-Cryst. Solids 352 (2006) 3069.

[24] Asha Rajiv, M Sudhakara Reddy, R Viswana Tha, Jayagopal Uchil, C Narayana Reddy, Bull. Mater.Sci., 38 (2015) 985.

[25] S. Sen, A. Ghosh, J. Non-Cryst. Solids 258 (1999) 29.

[26] N.H. Roy, J. Non-Cryst. Solids 15 (1974) 423.

[27] J.E. Shelby, J. Appl. Phys. 46 (1975) 193.

[28] H.E. Kissinger, Anal. Chem. 29 (1957) 1702.

[29] Lamia Heireche, Mohamed Heireche, Maamar Belhadji, J. Crystallization Process and Technology 4 (2014) 111.

[30] Andreia A.S. Lopes, Roque S. Soares, Maria M.A. Lima, Regina C.C. Monteiro, J. Applied Physics 115 (2014) 043516.

[31] S. Mahadevan, A. Giridhar, A.K. Singh, J. Non-Cryst. Solids 88 (1986) 11.

[32] J. Vazquez, P.L. Lopez-Alemany, P. Villares, R. Jimenez-Garay, J. Phys. Chem.Solids 61 (2000) 493.

[33] H.S. Chen, J. Non-Cryst. Solids 27 (1978) 257.

[34] W. Johnson, R. Mehl, Trans. Am. Inst. Min. Met. Eng. 135 **(**1939) 416.

[35] M. Avrami, J. Chem. Phys. 8 (1940) 212.

[36] M. Avrami, J. Chem. Phys. 9 **(**1941) 177.

[37] R.A. Ligeno, J. Vazquex, M. Casns-Ruix, R. Jirnenez-Caray, Thermochim. Acta 197 (1992) 319.

[38] C. Wagner, P. Villanes, J. Vazquex, R.R. Jirnenex-Caray, Mater. Lett.19 **(**1993) 370.

[39] Gao Yi Qun, W. Wang, F.Q. Zheng, X. Liu, J. Non-Cryst. Solids 81 (1986) 135.

[40] M. Shapaan, E.R. Shabaan, J. Phys. Chem. Solids 71 (2010) 1301.

[41] Essam R Shaaban, M. Shapaan, Yasser B Saddeek, J. Phys. Condens. Matter 20 (2008) 155108.

[42] Essam R. Shaaban, Ishu Kansal, M. Shapaan, J. Therm. Anal. Calorim. 98 (2009) 347.

[43] K. Matusita, S. Saka, J. Non-Cryst. Solids 38 (1980) 741.

[44] K. Matusita, T. Komatsu, R. Yokota, J. Mater. Sci. 19 (1984) 291.

[45] W. Lu, B. Yan, W. Huang, J. Non-Cryst. Solids 351 (2005) 3320.

[46] A.A. Joraid, S.N. Alamri, A.A. Abu-Sehly, J. Non-Cryst. Solids 354 (2008) 3380.

[47] A. Calka, A.P. Radlinski, Mater. Sci. Eng. 97 (1988) 241.

[48] K. Lu, J.T. Wang, Mater. Sci. Eng. A 133 (1991) 500.

[49] T. Ozawa, J. Therm. Anal. 2 (1970) 301.

[50] T. Ozawa, J. Therm. Anal. 31 (1986) 547.

[51] K. Majhi, K. Varma, J. Mater. Sci. 44 (2009) 385.